Journal of Power Sources 196 (2011) 10632–10639

Contents lists available at SciVerse ScienceDirect

Journal of Power Sources

journal homepage: www.elsevier.com/locate/jpowsour

Flooding of the diffusion layer in a polymer electrolyte fuel cell: Experimental and modelling analysis

A. Casalegno*, F. Bresciani, G. Groppi, R. Marchesi

Politecnico di Milano, Department of Energy, via Lambruschini 4, 20156 Milano, Italy

ARTICLE INFO

Article history:
Received 27 May 2011
Received in revised form 5 August 2011
Accepted 23 August 2011
Available online 30 August 2011

Keywords:
Fuel cell
PEFC
Diffusion layer
Flooding

ABSTRACT

Water management is widely investigated because it affects both the performance and the lifetime of polymer electrolyte fuel cells. Membrane hydration is necessary to ensure the high proton conductivity, but too much water can cause flooding and pore obstruction within the cathode gas diffusion layer and the electrode. Experimental studies prove that the characteristics of the diffusion layer have great influence on water transport; the introduction of a micro-porous layer between the gas diffusion layer and the electrode reduces flooding and stabilizes the performance of the fuel cell, although the reason is not fully explained. A quantitative method to characterize water transport through the diffusion layers was proposed in our previous work, and the present work aims to further understand the flooding phenomenon and the role of the micro-porous layer. The improved experimental setup and methodology allow an accurate and reliable evaluation of water transport through the diffusion layer in a wide range of operating conditions. The proposed 1D + 1D model faithfully reproduces the experimental data adopting effective diffusivity values in agreement with literature. The presented experimental and modelling analysis allows us to evaluate the influence of pore obstruction on the effective diffusivity, the overall transport coefficient and water flow through the diffusion layer, elucidating the effect of the micro-porous layer on fuel cell performance and operation stability.

1. Introduction

Polymer electrolyte fuel cells (PEFC) are very promising for CHP and automotive applications because of their high efficiency, very low emissions and modularity. However, they are still affected by technical problems that restrict their lifetime and performance. Water management in PEFC is one of the most investigated issues [1,2]. Indeed, polymer membrane hydration is necessary to ensure high proton conductivity, but too much water can cause flooding within the cathode gas diffusion layer (GDL) and the electrode. The flooding in the GDL or the electrode causes pore obstruction due to water condensation, which hinders oxygen transport from the distributor to the catalyst active sites and lowers the performance and the lifetime of the fuel cell [3]. Even with stack optimization, flooding can still occur during the real operation because of the variability in the operating conditions, which gives rise to transients in the water production and transport phenomena. In fact, water transport in PEFC is a result of several contributions such as electro-osmotic drag, diffusive and convective phenomena with phase transition and local water production. Reactant humidification is necessary to avoid membrane dehydration, and it has to be optimized considering the water transport properties of the porous layers. Experimental studies confirm that GDL characteristics have great influence on these phenomena [4]; the introduction of a micro-porous layer (MPL) between the GDL and the electrode reduces the flooding effect and stabilizes the fuel cell performance although the reason is not fully explained [5–7]. Despite its arguable relevance, GDL flooding is not exhaustively investigated in the literature; actually, no common methodologies to compare the different properties of GDL water transport are available. In most experimental studies, these properties are investigated by characterising two physical indicators during the fuel cell operation [8–13]: the overall performance and the water flow at the cathode outlet. Under these conditions, the interplay of different phenomena complicates the interpretation of the results. In the literature, the direct investigations of the water transport and the flooding mechanism in GDL are generally more qualitative than quantitative. For example, they are investigated through infrared thermography during the fuel cell operation, showing that the flooded area is warmer than the not flooded one [14]. In some studies, the water dynamics inside the fuel cell are characterised

* Corresponding author. Tel.: +39 0223993912; fax: +39 0223993913.
E-mail address: andrea.casalegno@polimi.it (A. Casalegno).

0378-7753/$ – see front matter © 2011 Elsevier B.V. All rights reserved.
doi:10.1016/j.jpowsour.2011.08.094

Nomenclature

C	local concentration [mol m^{-3}]
$\hat{C}$	local concentration in the gas phase [mol m^{-3}]
v	velocity of the flow [m s^{-1}]
P	pressure [Pa]
x	axial direction [m]
L	channel length [m]
a	channel width and height [m]
T	GDL temperature [K]
R	universal gas constant [J mol^{-1} K^{-1}]
t	thickness [m]
D	diffusivity [m^2 s^{-1}]
k	local water transport coefficient [m s^{-1}]
h	convective mass transport coefficient [m s^{-1}]
FC	local flooding coefficient
F	2D factor
$\dot{N}$	molar flow [mol s^{-1}]
$\dot{V}$	volumetric flow [m^3 s^{-1}]

Subscripts

2p	relative to a two-phase flow
d	relative to a dry flow
h	relative to a humid flow
H_2O	relative to water
air	relative to air
eff	effective
overall	including possible pore obstruction
sat	relative to saturation
in	at the inlet
out	at the outlet

superscripts

h	relative to a humid flow
d	relative to a dry flow
MPL	relative to MPL
GDL	relative to GDL
GDL + MPL	relative to GDL with MPL
tot	total
diff	diffusive
perm	permeative

using optical techniques such as neutron imaging [15,16] and X-ray imaging [17,18], providing evidence for the water cluster formation and the preferential liquid pathways in the porous material.

In [19], Casalegno et al. proposed a quantitative method to characterise the water transport through the gas diffusion layers by introducing a global water transport coefficient that allows a comparison of different GDLs. The porous media were analysed in realistically simulated operating conditions, which were obtained by supplying the two GDL faces with humid and dry airflows. The measurements showed that a reduction in water transport occurred when there was a significant amount of liquid water, which could be attributed to flooding, and that the MPL had a beneficial influence on the flooding effect.

This work aims to further understand the flooding phenomenon and the MPL role through the following goals:

- improving the experimental setup to achieve a wider range of operating conditions;
- developing a 1D + 1D model, which is validated by the experimental results.

2. Experimental methodology

2.1. Experimental setup

The experimental approach, as reported in detail in [19], consists of supplying the two GDL faces with a humid air flow and a dry air flow in a co-current configuration so that the water flows from the humid side to the dry side by diffusion. The pressure difference between the two flows has to be minimized to make permeation negligible compared to diffusion. Fig. 1 shows schematics of the experimental setup. The water flux through the dry side of the GDL is calculated as follows:

$$\dot{N}^{GDL}_{H_2O} = \dot{V}^{d}_{out} \cdot C^{d}_{H_2O,out} - \dot{V}^{d}_{in} \cdot C^{d}_{H_2O,in} \quad (1)$$

The experimental setup is improved with the following design:

- a more effective evaporator, which allows a more uniform and stable water evaporation in dry air, to decrease the variability and the uncertainty of the relative humidity measurement;
- an improved temperature control system, which permits a more accurate temperature control for different components (the typical deviation is less than 0.1 °C) and an extension of the maximum allowed temperature of the humidity sensors (up to 110 °C).

These modifications allow a significant extension of the operating condition range: the maximum inlet water concentration is increased from 11.5 mol m^{-3} to 15 mol m^{-3}, permitting the investigation of more intensive flooding conditions.

The gas diffusion layer, of which the surface area that is exposed to the fluxes is 4.2 cm × 4.2 cm, is contained between two graphite distributors, where the channels for the humid and the dry airflows have been grooved (both distributors have a triple serpentine channel with a square section: depth 0.8 mm, width 0.8 mm, length 700 mm). The graphite distributors are held together with two stainless steel plates using 8 retaining bolts that are closed with a controlled torque of 12 ± 0.5 N m. The thickness of the compressed GDL is maintained constant at approximately 330 μm, to adopt the appropriate gaskets. A slot in one of the steel plates accommodates a calibrated thermocouple, which is connected with a temperature controller and a data acquisition system. Two electrical heaters, which are connected to the temperature controller, are placed within the steel plates to fully control the temperature of the assembly. Because the heat capacity of the plates is much greater than that of the graphite distributors and the GDL, high temperature stability is attained. The rates of the airflows are controlled and measured by two calibrated flow controllers. The air humidification is obtained by adding bi-distilled water to the air stream with a precise peristaltic pump. Air pressure, temperature and humidity are measured at GDL inlets and outlets with the calibrated instruments. At the dry outlet, a condenser permits us to reduce and to control the water content; thus, the airflow and the temperature are measured using a calibrated flow meter assuming saturation.

2.2. Results reliability evaluation

Table 1 reports the range and the measurement uncertainty of all measured parameters. These quantities were acquired at a frequency of 1 Hz for 1500 s in steady state conditions. The data were processed with a robust method for outlier elimination. The representative values of each parameter were obtained as the average of the first 1000 elements among the remaining ones.

The uncertainty of the experimental setup was evaluated for the measurements of both the water concentrations and the water flow through the GDL. The global uncertainty of the experimental

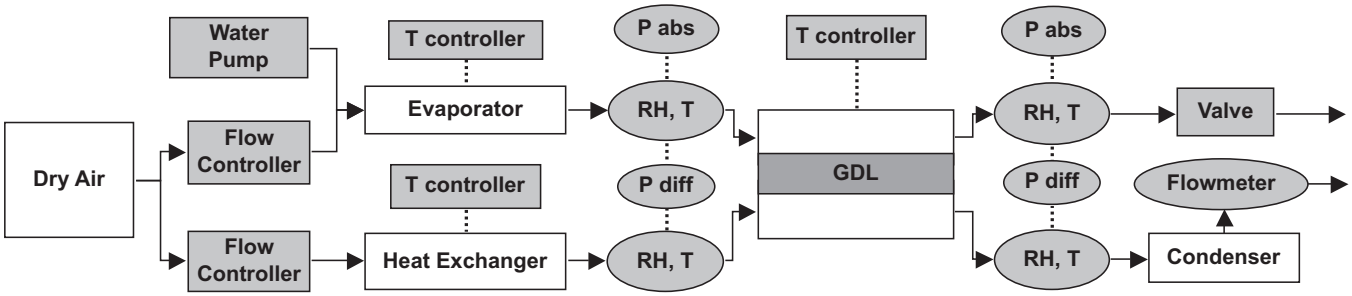

Fig. 1. Experimental setup.

setup was estimated by combining the uncertainties of the different instruments as shown in [20]. The estimated values are 7% for the water concentration and 8% for the water flow through the GDL.

The reproducibility of the results was verified by repeating every experimental measurement on three different days. These experimental results were compared using ANOVA. This analysis confirmed that the differences between the days are not statistically significant if the account measurement uncertainty is taken into account; thus, the experimental results can be considered reproducible.

As previously stated, the relative humidity at a humid outlet is measured to verify the mass conservation. In the investigated conditions, the difference between the inlet and the outlet water flows is lower than 5%, which is less than measurement uncertainty.

The last hypothesis that supports this experimental investigation concerns the different contributions to water transport through GDL; permeation is considered negligible, and thus mass transport occurs mainly by diffusion:

$$\begin{cases} \dot{N}^{\text{tot}}_{H_2O} = \dot{N}^{\text{diff}}_{H_2O} + \dot{N}^{\text{perm}}_{H_2O} \\ \dot{N}^{\text{perm}}_{H_2O} \sim 0 \end{cases} \quad (2)$$

This assumption was validated through apposite experimental tests: in Fig. 2, the water flow through the GDL is plotted versus the mean pressure difference across the GDL $\overline{\Delta P}$, which is defined as:

$$\overline{\Delta P} = \frac{\Delta P_{\text{in}} + \Delta P_{\text{out}}}{2} \quad (3)$$

The presented data were obtained with constant temperature and constant water inlet concentration. The results show the influence of the mean pressure difference across the GDL on water transport. When the humid side is pressurized, the air–water mixture is forced to cross the GDL due to permeation from the humid side to the dry side, increasing the total water transport, and vice versa when the dry side is pressurized. A considerable difference, over 15%, is obtained by imposing a pressure difference of 500 Pa across the GDL, confirming a considerable permeation contribution.

If instead, during characterisation of water transport through GDL, the pressure difference value was maintained lower than 100 Pa, then the maximum variation in water transport is only 4%. Therefore, considering the global uncertainty of water flow through GDL (8%), the permeation contribution on water transport can be considered negligible.

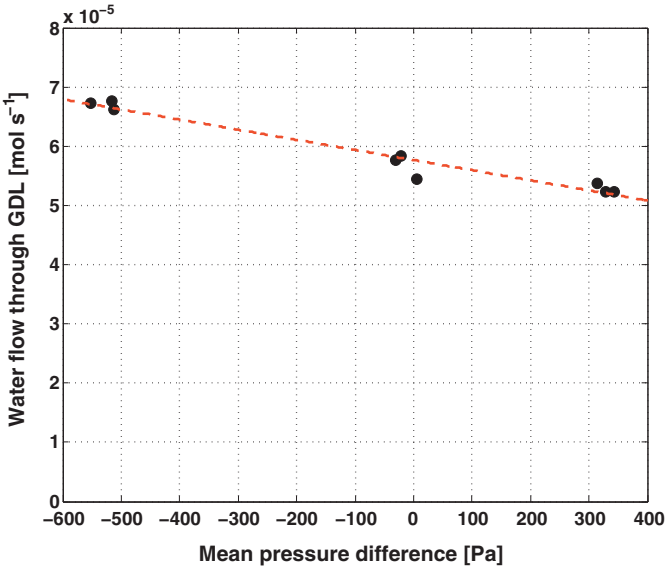

Fig. 2. Influence of the differential pressure on the water flux through the GDL.

3. Experimental results

Table 2 summarizes the physical properties of the two investigated commercial GDLs. The only morphological difference between these two porous media is the presence of a micro-porous layer that influences the thickness, areal weight and air permeability. The experimental characterisation of the GDL with MPL is carried out by posing the MPL on the humid side to appraise the consequential pore obstruction just in the MPL.

Fig. 3 shows the water flow through the GDL, with and without MPL, as a function of the total water concentration at the humid inlet. The experimental results point out two distinct trends for each GDL relative to the two investigated temperature conditions. At the higher temperature, a linear trend of the water flux is detected by increasing the inlet water concentration up to the

Table 1
Range and uncertainty of the measured parameters.

	Range	Uncertainty
Inlet air flow [g min^{-1}]	1.94–2.42	0.7% + 0.006
Pump water flow [g min^{-1}]	0.2–0.5	1%
Absolute pressure [kPa]	108–125	0.2
Differential pressure [Pa]	10–100	20
Relative humidity [%]	26–80	1.5% + 1.5% of measure
Temperature [K]	333–343	0.1

Table 2
GDL characteristics.

	GDL with MPL	GDL without MPL
Type	Carbon fibre paper	Carbon fibre paper
Thickness (uncompressed) [μm]	415	400
MPL thickness [μm]	50	–
PTFE content	10%	10%
Surface [cm^2]	18.14	18.14
Areal weight [g m^{-2}]	145	901
Air permeability [cm^3 cm^{-2} s^{-1}]	1.45	85

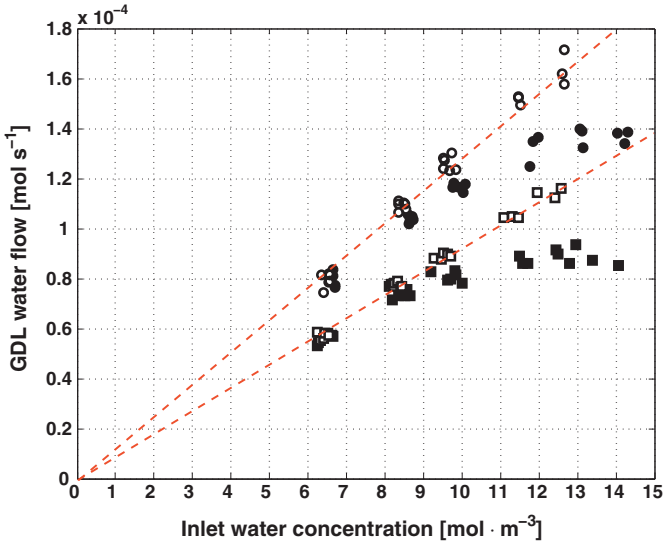

Fig. 3. Water flux as a function of the inlet water concentration through GDL with MPL (square) and GDL without MPL (circle), at 333 K (black) and 343 K (white).

maximum investigated value, 13 mol m^{-3}, which is 1.2 times the saturation value.[1] At the lower temperature, the results show a deviation from linearity for the inlet water concentration in the range of 8.5–14.5 mol m^{-3}, corresponding to 1.2–2 times the saturation value. In this range, the water condensation in the channels and within the GDL pores, the so-called flooding phenomenon, determines a limitation in the water flux across the GDL, as previously reported in [19].

By improving the investigated operating condition range, we can more exhaustively characterise this deviation from linearity. At 60 °C, the water flux tends toward an approximately constant value when the inlet water concentration is increased up to twice the saturation value. A similar trend could be reasonably expected at higher temperatures, if the suitably inlet water concentration is increased.[2] This profile can be related to two phenomena: the saturation of air in the humid channel and the obstruction of the GDL pores. Indeed, the air saturation limits the vapour concentration gradient across the GDL, the diffusion driving force, which contributes to restraining the water flow, in addition to the pore obstruction. The available experimental data do not permit the quantification of each contributing factor; therefore, a suitable modelling analysis, as reported in the next section, is carried out to achieve a deeper understanding.

The analogous considerations are valid for GDL with MPL; moreover, the results prove that this extra layer has a great influence on the vapour phase transport by increasing the GDL mass transport resistance: the water flow at equal inlet water concentration is generally 25–30% less. The overall mass transport resistance is increased substantially by the presence of the MPL, which confirms the previous results [19]. Despite the low thickness, the MPL transport resistance is comparable or even higher than the resistance of the GDL bulk material, mainly due to the Knudsen diffusion contribution. A detailed comparison with diffusivity data available in literature is reported in the following analysis.

[1] The saturation concentration at 60 °C and 70 °C are 7.14 and 10.85 mol m^{-3}, respectively, and beyond these values, the humid stream is actually a two-phase flow.

[2] In some practical conditions, intensive flooding can also be present at higher temperatures, especially in direct methanol fuel cell (DMFC), and water concentration at the cathode outlet can be higher than 2 times saturation value at either 70 °C or 80 °C [3].

4. Model description

The developed model is not an exhaustive description of the complex phenomena that occur in the analysed system, but it is a reliable tool to interpret the experimental data and to increase the understanding of the water transport mechanisms in GDL by evaluating the influence of pore obstruction.

4.1. The equation system

A 1D + 1D model is developed to describe the steady state water transport through the gas diffusion layer and to estimate local quantities, such as the water concentration and the effective diffusivity. The model is based on the following assumptions:

- the GDL properties are homogeneous;
- the domain is considered isothermal;
- air is considered a single chemical species;
- the gas and the gas mixture are considered ideal;
- the channels have a square section;
- the serpentine flow field is simplified to straight channels[3];
- the plug flow is considered in the channels;
- the humid and dry flows have the same local pressure;
- the pressure drop along the channel has a linear distribution;
- permeation and convection are neglected within the GDL.

The model is a differential-algebraic system, composed of 7 equations and is solved with the Matlab® software.

The first and second equations describe water flux in the dry and humid channels, respectively:

$$\frac{\partial(v^{d} \cdot C^{d}_{H_2O})}{\partial x} = \frac{k}{a} \cdot (\hat{C}^{h}_{H_2O} - C^{d}_{H_2O}) \quad (4)$$

$$\frac{\partial(v^{h} \cdot C^{h}_{H_2O})}{\partial x} = -\frac{k}{a} \cdot (\hat{C}^{h}_{H_2O} - C^{d}_{H_2O}) \quad (5)$$

where k is the local transport coefficient, a is the channel width, and the water vapour concentration $\hat{C}^{h}_{H_2O}$ the humid channel is defined as the minimum value between $C^{h}_{H_2O}$ and the saturation value C_{sat}:

$$\hat{C}^{h}_{H_2O} = \min(C^{h}_{H_2O}, C_{sat}) \quad (6)$$

The third and fourth equations describe air flux in the dry and humid channels, respectively:

$$\frac{\partial(v^{d} \cdot C^{d}_{air})}{\partial x} = \frac{k}{a} \cdot (C^{h}_{air} - C^{d}_{air}) \quad (7)$$

$$\frac{\partial(v^{h} \cdot C^{h}_{air})}{\partial x} = -\frac{k}{a} \cdot (C^{h}_{air} - C^{d}_{air}) \quad (8)$$

The fifth and sixth equations describe the gas phase concentrations in the dry and humid channels, respectively:

$$C^{d}_{H_2O} + C^{d}_{air} = \frac{P}{R \cdot T} \quad (9)$$

$$\hat{C}^{h}_{H_2O} + C^{h}_{air} = \frac{P}{R \cdot T} \quad (10)$$

where T is the domain temperature and R is the universal gas constant.

The last equation describes the linear pressure distribution along the channels:

$$\frac{\partial P}{\partial x} = -\frac{P_{in} - P_{out}}{L} \quad (11)$$

[3] The effect of channel bends is taken into account evaluating convective mass transport coefficient, as explained in the following.

where L is the total channel length, and P_{in} and P_{out} are the pressures at the GDL inlet and outlet.

4.2. Evaluation of mass transport coefficients

Assuming the diffusive mass transport through the GDL, the local transport coefficient k in the investigated setup is determined by both the GDL diffusivity and the convective mass transport coefficients of channels. Considering diffusive and convective mass transport notions [21], it can be expressed as follows:

$$\frac{1}{k} = \frac{1}{h_h} + \frac{1}{F \cdot D_{overall}} + \frac{1}{h_d} \quad (12)$$

where h_h and h_d are the convective mass transport coefficients for the humid and dry channels, t is the GDL thickness, $D_{overall}$ is the GDL overall diffusivity, and F is a correction factor to consider 2D diffusion effects within GDL. The evaluation of these parameters is reported in details later on.

4.2.1. Convective mass transport coefficient, h

The following analysis is valid for the flows with water concentration below the saturation point; when local flooding coefficient FC is less than 1:

$$FC = \frac{C^h_{H_2O}}{C_{sat}} < 1 \quad (13)$$

The estimation of the convective mass transport coefficient is based on three considerations:

- the Lewis analogy is valid: the mass transport boundary layer can be described by the thermal boundary layer models;
- the flow is completely mixed at every bend of the channel, determining a subsequent developing region;
- the channel can be modelled as a square tube with one exchanging face.

The correlations to determine the convective coefficients for a not-fully developed flow in this domain are not available in the literature. Therefore, despite its limited rigor and precision, the following method is adopted to approximately evaluate h:

1. the flow regime and thermodynamic properties are evaluated according to [21];
2. the influence factor of the developing region on h in a square tube with all exchanging surfaces is calculated for both a constant flux and a constant surface concentration, and the correlations are reported in [22,23];
3. the value of h for the fully developed flows in the square tubes with only one exchanging surface is calculated for both a constant flux and a constant surface concentration the correlations are reported in [24];
4. the value of h for the developing flows in the square tubes with only one exchanging surface is estimated by increasing the value calculated at point 3 by the factor evaluated at point 2.

The dimensionless groups evaluated to calculate the mass transport convective coefficients are summarized in Table 3.

Fig. 4 shows the influence of several parameters on the convective coefficient,[4] which is affected as follows:

Table 3
Dimensionless groups at 333 K.

	Constant concentration		Constant flux	
	Humid side	Dry side	Humid side	Dry side
Re	700–900	650–850	700–900	650–850
Flow regime	Laminar	Laminar	Laminar	Laminar
Sc	0.69–0.75	0.62–0.65	0.69–0.75	0.62–0.65
Le	0.7–0.76	0.79–0.82	0.7–0.76	0.79–0.82
$Sh_{dev\ 4\ faces}$	2.98	2.98	3.61	3.61
$Sh_{notdev\ 4\ faces}$	3.41–3.46	3.37–3.44	3.98–4.02	3.95–4.01
$Sh_{dev\ 1\ face}$	2.437	2.437	2.712	2.712
$Sh_{notdev\ 1\ face}$	2.79–2.83	2.76–2.82	2.99–3.02	2.97–3.01

- poorly by the velocity; thus, this effect is neglected;
- considerably by a constant concentration or a constant flux; because the real system is an intermediate case, the mean value is adopted;
- considerably by the temperature.

For these reasons, the adopted values of the convective mass transport coefficient for FC < 1 are:

$$\begin{cases} h_h = h_d \\ h_h = 0.115\ \text{m s}^{-1} & \text{if } T = 333\,\text{K} \\ h_h = 0.12\,\text{m s}^{-1} & \text{if } T = 343\,\text{K} \end{cases} \quad (14)$$

The correlations to determine the Sherwood number in the two-phase flow conditions, with FC > 1, are not available in the literature. Considering the thermal analogy and the typical flow patterns, mainly the droplet and the film flows [25], it is reasonable to expect the convective coefficient to be enhanced by roughly one order of magnitude, but the quantification is not reliable. Therefore, a sensitivity analysis on k is carried out with the two-phase convective coefficient h_{2p} varied from 3 to 100 times h_h.

4.2.2. 2D effect factor, F

The factor F is introduced to take into account the 2D geometric effect on diffusion through the GDL due to the investigated flow field, which is otherwise neglected with a one-dimensional lumped model. The local fluxes through the GDL, considering and neglecting 2D effect, are estimated by simulating the system in typical conditions using COMSOL Multiphysics®. In Fig. 5, F is defined as the ratio of the flux through the whole GDL (domain A + B) to the flux

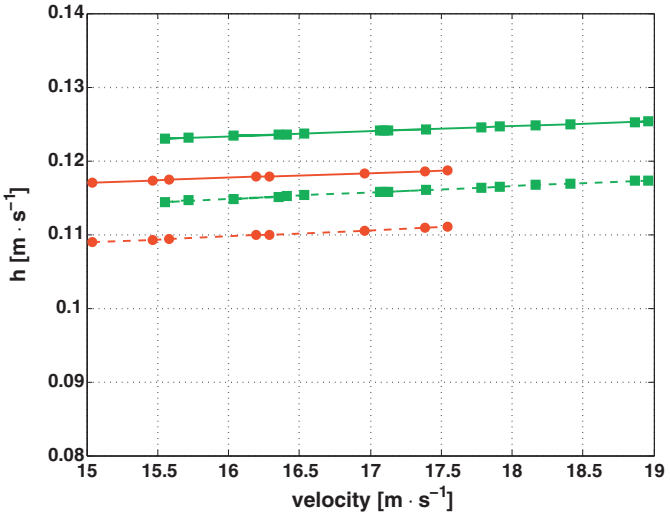

Fig. 4. Mass transport convective coefficient as a function of the gas velocity at 333 K (circle) and 343 K (square), considering the constant flux (line) and the constant concentration (dotted line) schemes.

[4] The effect of flow composition on convective transport coefficient is not reported, because negligible.

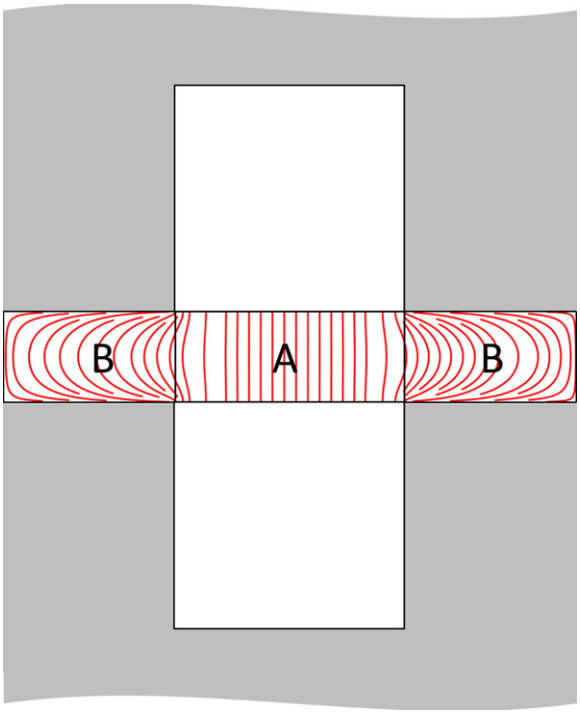

Fig. 5. Cross-sectional view of the investigated domain; diffusive flux lines are reported in the GDL section.

through just the fraction of the GDL between the channels (domain A). The F value that results from the investigated geometry is 1.27.

4.2.3. Effective diffusivity, D_{GDL}

As previously stated, the local GDL effective diffusivity is affected by the consequential pore obstruction in the presence of the water liquid phase. To consider this phenomenon, a general model is proposed, where $D_{overall}$ decreases as a function of the water liquid concentration[5]:

$$\begin{cases} D_{overall} = D_{eff} \cdot \left(\dfrac{T}{333}\right)^{1.75} & \text{if } FC \le 1 \\ D_{overall} = [D_{eff} - C_1 \cdot (C^{h}_{H_2O} - C_{sat})^{C_2}] \cdot \left(\dfrac{T}{333}\right)^{1.75} & \text{if } FC > 1 \end{cases} \quad (15)$$

D_{eff}, C_1 and C_2 are unknown parameters, characteristic of the investigated GDL at the reference temperature of 333 K; in the next section, they are determined through calibration with experimental data and compared with results reported in the literature. These relations provide a nonlinear diffusivity dependence on the water liquid concentration when the overall water concentration exceeds the water saturation value. The effective diffusivity is considered exponentially dependent on the temperature [21].

5. Modelling results

5.1. Model validation

A calibration procedure is carried out in Matlab® to determine the value of the 3 fitting parameters D_{eff}, C_1 and C_2 while varying the value of h_{2p}. The calibration procedure includes minimising the residuals between the model estimation and the experimental results in the complete investigated range of operating conditions,

[5] Equal to the difference between total water concentration and saturation vapour concentration.

Table 4
Obtained fitting parameters values.

	$h_{2p} = 3h_m$	$h_{2p} = 10h_m$	$h_{2p} = 100h_m$
GDL without MPL			
D_{eff} [m^2 s^{-1}]	1.599e^{-5}	1.596e^{-5}	1.595e^{-5}
C_1	1.21e^{-6}	2.59e^{-6}	3.10e^{-6}
C_2	0.976	0.581	0.491
GDL with MPL			
D_{eff} [m^2 s^{-1}]	5.559e^{-6}	5.559e^{-6}	5.559e^{-6}
C_1	4.24e^{-8}	2.75e^{-7}	3.59e^{-7}
C_2	0.232	0.027	0.019

which are 51 measures for each GDL. The residuals between the model and the experimental results are always one order of magnitude lower than measurement uncertainty, independently of the adopted value of h_{2p}. Table 4 reports the obtained values of the fitting parameters. It is worth noting that the variation of D_{eff} is very limited by different values of h_{2p}, confirming that the uncertainty on the latter does not affect considerably the determination of the first by calibration.

To evaluate the reliability of the obtained results, a comparison with the data reported in the literature is reported.

GDL with MPL has been considered a two-layer structure; the effective diffusivity of the sole MPL can be obtained by the following relation:

$$D_{eff}^{GDL+MPL} = \frac{t^{GDL+MPL}}{t^{MPL}/D_{eff}^{MPL} + t^{GDL}/D_{eff}^{GDL}} \quad (16)$$

Table 5 summarizes the effective diffusivity values of GDL and MPL at FC < 1 and 333 K that are available in the literature, as obtained from the correlations in [21], assuming pore radius, porosity and the eventual Knudsen effects [26,27], and from the experimental results [28]. No data obtained for the flooding conditions are available in the literature; thus, no comparison is possible.

The effective diffusivity values obtained by model calibration are in agreement with the values in the literature for both GDL with MPL and GDL without MPL. Subsequently, the model is considered accurate and reliable in reproducing experimental data in the investigated conditions.

5.2. Flooding analysis

In Fig. 6, the effective diffusivity of the investigated layers is reported as a function of FC. When this quantity is higher than 1, the

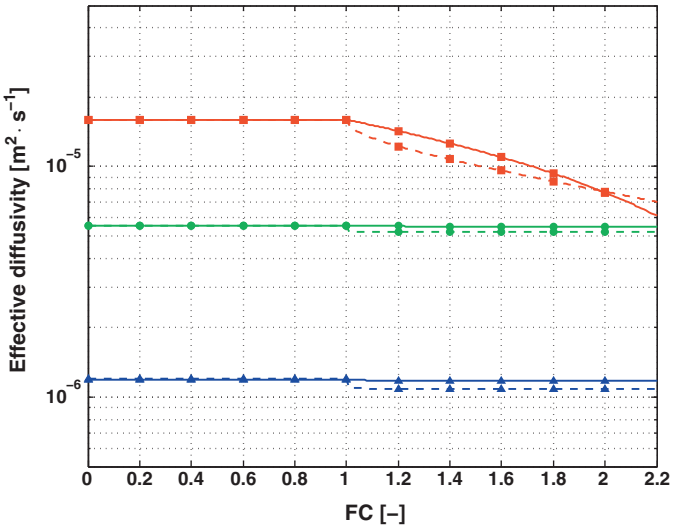

Fig. 6. Effective diffusivity as a function of FC for GDL without MPL (square), GDL with MPL (circle), and MPL (triangle), considering $h_{2p} = 3h_h$ (line) and $h_{2p} = 100h_h$ (dotted line).

Table 5
Effective diffusivity of GDL.

	Thickness [μm]	Pore radius [μm]	Porosity ε	D_{eff} [$m^2 s^{-1}$]		
				Correlation [21]	Experiments [28]	Present work
GDL without MPL	330	25–60	0.6–0.8	$9.13e^{-6}$–$1.9e^{-5}$	$7.8e^{-6}$–$1.6e^{-5}$	$1.59e^{-5}$
MPL	50	0.08–0.5	0.3–0.5	$8.03e^{-7}$–$1.55e^{-6}$	–	$1.195e^{-6}$
GDL with MPL	330	–	–	$2.58e^{-6}$–$1.26e^{-5}$	–	$5.56e^{-6}$

effective diffusivity of GDL with and without MPL decreases proportionally with FC and the liquid water concentration. This behaviour confirms that the presence of the liquid water phase determines a substantial pore obstruction. In the case of GDL without MPL, the reduction is dramatically higher than in the case with MPL. As expected, the smaller pore radius and the higher hydrophobicity of the MPL significantly reduce pore obstruction. When the value of h_{2p} is varied from 3 to 100 times h_h, the results are essentially unaffected. In general, this change determines a slightly higher diffusivity reduction and a decrease in the exponent C_2. It is worth noting that in the case of GDL without MPL, this parameter is much nearer to unity than in the other case, especially for h_{2p} equal 3 times h_h, where the effective diffusivity decreases linearly with the liquid water concentration. Further experimental work is necessary to obtain more precise evaluations of the convective coefficients and consequently a more accurate estimation of the diffusivity reduction.

The effective diffusivity of MPL is calculated from the previously discussed diffusivities, attributing pore obstruction to the sole MPL and neglecting this phenomenon in the bulk GDL material. Comparing GDL and MPL at FC equal to 2.2, the diffusivity reductions are noticeably different: 56–62% and 1.5–7%, respectively. Subsequently, the effective diffusivities of GDL with and without MPL assume very similar values with FC of about 2.2: the higher mass transport resistance due to the MPL presence is compensated by a less effective pore obstruction. This result is consistent with the beneficial MPL influence on the PEMFC performance in severe flooding conditions, which was reported in the literature [3,11–13].

In Fig. 7, the local transport coefficient k, defined in Eq. (12), is reported as a function of FC; for clarity, the single intermediate value of 10 is adopted for h_{2p} in the following analysis. When FC is increased above 1, the coefficient k for the GDL has an initial increase, due to the enhanced h value, followed by a decrease caused by a reduction in D_{eff}. The behaviour of the GDL with MPL is different: k increases approximately up to a constant value. Thus, in the latter case, the reduction of D_{eff} has a limited influence on the overall transport coefficient. To show the effects of diffusivity reduction more clearly, the k values calculated while omitting pore obstruction, i.e., with C_1 equal to zero, are reported in Fig. 7 as dotted lines. The difference between the solid and the dotted lines may be attributed to pore obstruction: this phenomenon strongly affects the k value for GDL without MPL, while it is not so relevant in the other case. This consideration may also help reasoning the more stable PEFC operation that introduces the MPL, which is widely reported in the literature [3]: pore hindrance is an unsteady phenomenon; thus, the local transport coefficient k varies intermittently from a minimum to a maximum value, respectively with and without pore obstruction. The fluctuation of k is much more limited for the GDL with MPL; hence, the introduction of the latter layer increases the robustness to the liquid water presence.

Both the experimental results and the model estimations of the water transport through the GDL without and with MPL are reported in Figs. 8 and 9. The previous considerations are also valid for the water flux, although it is a global quantity because of its intimate correlation with the local transport coefficient k. In these figures, the effect of pore obstruction can be evaluated by comparing the difference between the solid lines (modelling results with pore obstruction) and the dotted lines (results without pore obstruction). It is worth noting that the deviation from linearity has different origins for GDLs with and without MPL: in the former case, it is mainly due to the saturation threshold (Fig. 9), while in the latter case, it is predominantly caused by pore obstruction (Fig. 8). The comparisons between the modelling and the experimental results confirm once again the validity of the proposed interpretation and emphasise the influence of pore obstruction on water transport through the investigated GDL.

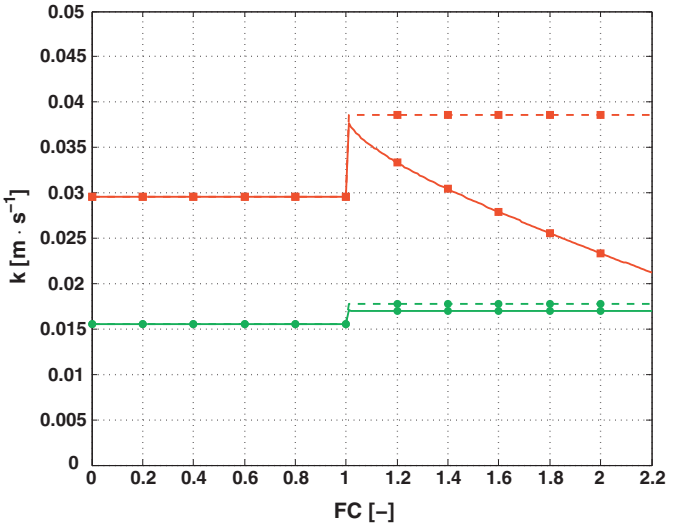

Fig. 7. Overall mass transport coefficient as a function of FC for GDL without MPL (square) and GDL with MPL (circle) with $h_{2p} = 10h_h$, including (line) and omitting (dotted line) pore obstruction.

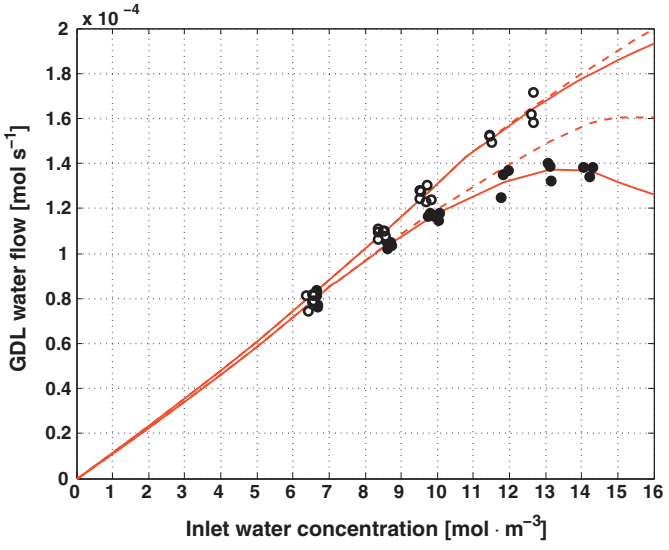

Fig. 8. Experimental water flux through GDL without MPL at 333 K (black circle) and 343 K (white circle), compared with the modelling results including (line) and omitting (dotted line) pore obstruction.

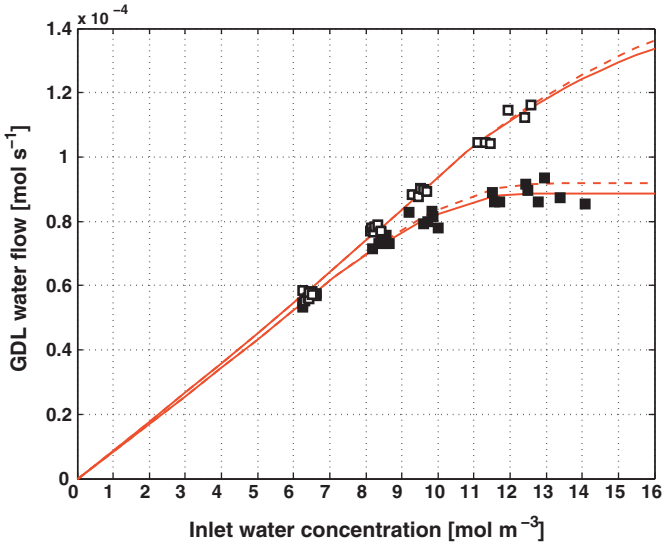

Fig. 9. Experimental water flux through GDL with MPL at 333 K (black square) and 343 K (white square) compared with the modelling results, including (line) and omitting (dotted line) pore obstruction.

6. Conclusions

The proposed combined experimental and modelling approach permits a reliable evaluation of water transport through the GDL and an accurate reproduction of the experimental data, using the developed 1D + 1D model, which adopts the effective diffusivity values in agreement with the literature. The correlations to describe quantitatively the GDL diffusivity reduction caused by pore obstruction are proposed for both GDL with and without MPL, contributing to elucidate and quantify the MPL influence on water transport. The analysis confirms that pore obstruction strongly affects GDL without MPL but is not so relevant for GDL with MPL, according to the literature. The reported deviation from linearity of the water transport through the GDL, expressed as a function of the inlet water concentration, has different origins for GDLs with and without MPL: it is mainly due to the saturation threshold in the first case, while it is predominantly caused by pore obstruction in the second case. Moreover, the investigation elucidates that the fluctuation of water transport due to pore obstruction is much more limited for the GDL with MPL. Thus, the introduction of this layer increases the robustness of PEFC or DMFC to the presence of liquid water and induces a more stable operation, which explains some experimental results reported in the literature.

Acknowledgement

The funding for this work is from Fondazione Cariplo under agreement no. 2007.5543.

References

[1] F.A. De Bruijn, V.A.T. Dam, G.J.M. Janssen, Fuel Cells 8 (2008) 3–22.
[2] N. Yousfi-Steiner, P. Mocoteguy, D. Candusso, D. Hissel, A. Hernandez, A. Aslanides, J. Power Sources 183 (2008) 260–274.
[3] H. Li, Y. Tang, Z. Wang, Z. Shi, S. Wu, D. Song, J. Zhang, K. Fatih, J. Zhang, H. Wang, Z. Liu, R. Abouatallah, A. Mazza, J. Power Sources 178 (2008) 103–117.
[4] L. Cindrella, A.M. Kannan, J.F. Lin, K. Saminathan, Y. Ho, C.W. Lin, J. Wertz, J. Power Sources 194 (2009) 146–160.
[5] U. Pasaogullari, C. Wang, Electrochim. Acta 49 (2004) 4359–4369.
[6] H.K. Atiyeh, K. Karan, B. Peppley, A. Phoenix, E. Halliop, J. Pharoah, J. Power Sources 170 (2007) 111–121.
[7] T. Kitahara, T. Konomi, H. Nakajima, J. Power Sources 195 (2010) 2202–2211.
[8] C. Quick, D. Ritzinger, W. Lehnert, C. Hartnig, J. Power Sources 190 (2009) 110–120.
[9] F. Barbir, H. Gorgun, X. Wang, J. Power Sources 141 (2005) 96–101.
[10] J. Chen, T. Matsuura, M. Hori, J. Power Sources 131 (2004) 155–161.
[11] J. Benziger, T. Whitaker, E. Kimball, I.G. Kevrekidis, ECS Trans. 12 (2008) 67–79.
[12] S. Shimpalee, U. Beuscher, J.W. Van Zee, Electrochim. Acta 52 (2007) 6748–6754.
[13] C. Lim, C.Y. Wang, Electrochim. Acta 49 (2004) 4149–4156.
[14] A. Hakenjos, H. Muenter, U. Wittstadt, C. Hebling, J. Power Sources 131 (2004) 213–216.
[15] R. Satija, D.L. Jacobson, M. Arif, S.A. Werner, J. Power Sources 129 (2004) 238–245.
[16] P. Boillat, D. Kramer, B.C. Seyfang, G. Frei, E. Lehmann, G.G. Scherer, A. Wokaun, Y. Ichikawa, Y. Tasaki, K. Shinohara, Electrochem. Commun. 10 (2008) 546–550.
[17] P.K. Sinha, P. Halleck, C. Wang, Electrochem. Solid-State Lett. 9 (2006) A344–A348.
[18] C. Hartnig, I. Manke, R. Kuhn, S. Kleinau, J. Goebbels, J. Banhart, J. Power Sources 188 (2009) 468–474.
[19] A. Casalegno, L. Colombo, S. Galbiati, R. Marchesi, J. Power Sources 195 (2010) 4143–4148.
[20] ISO, 1993, Guide to Expression of Uncertainty in Measurement, BIPM, IEC, IFCC, ISO, IUPAC, IUPAP, OIML International Organization for Standardization, Env. 13005: 1999. led., Corrected and Reprinted 1995.
[21] R.H. Perry, D.W. Green, Perry's Chemical Engineer's Handbook, McGraw-Hill, 1999.
[22] W.M. Kays, Convective Heat and Mass Transfer, McGraw-Hill, 1993.
[23] S. Kakac, R.K. Shah, W. Aung, Handbook of Single-phase Convective Heat Transfer, Wiley, 1987.
[24] R.K. Shah, A.L. London, Adv. Heat Transfer (Suppl. I) (1978).
[25] I.S. Hussaini, C.-Y. Wang, J. Power Sources 187 (2009) 444–451.
[26] Z. Zhan, J. Xiao, D. Li, M. Pan, R. Yuan, J. Power Sources 160 (2006) 1041–1048.
[27] N. Zamel, X. Li, J. Shen, Energy Fuels 23 (2009) 6070–6078.
[28] R. Fluckiger, S.A. Freunberger, D. Kramer, A. Wokaun, G.G. Scherer, F.N. Buchi, Electrochim. Acta 54 (2008) 551–559.